THE PENNSYLVANIA STATE UNIVERSITY
SCHREYER HONORS COLLEGE

DEPARTMENT OF BIOMEDICAL ENGINEERING

DEVELOPMENT OF A MULTI-LAYERED MICRO-PATTERNED ELECTROSPUN MESH FOR HERNIA REPAIR

SARA ORR
FALL 2015

A thesis
submitted in partial fulfillment
of the requirements
for a baccalaureate degree Bioengineering
with honors in Bioengineering

Reviewed and approved* by the following:

Jian Yang
Professor of Biomedical Engineering
Thesis Supervisor

William Hancock
Professor of Biomedical Engineering
Honors Adviser

Yong Wang
Associate Professor of Biomedical Engineering
Thesis Committee Member

* Signatures are on file in the Schreyer Honors College.

ABSTRACT

Hernia repair is one of the most common surgeries in the world, with an estimated 20 million repairs performed each year[1]. With a lifetime risk of 27% for men and 3% for women in the United States and more than 990,000 abdominal wall hernias repaired every year, it is the second-most common surgical procedure in the country[2].

In this study, we developed a novel hernia mesh in aim to reduce chronic pain and recurrence. The ideal mesh requires not only a soft nature and in vivo biodegradability, but also a gradual transfer of mechanical loads upon implantation to promote healing. The first goal of this project was to fabricate a novel biodegradable electrospun mesh with an elegant structural design to meet the mechanical requirements necessary for successful hernia repair. The second goal of this project was to design the electrospun mesh to allow for faster cell infiltration and integration into the host tissue to improve the biological properties of meshes used in hernia repair.

We developed a novel design for a multi-layered micro-patterned electrospun hernia mesh assembly that could also be used as a wound dressing. Biodegradable micro/nano-fibrous meshes, using polycaprolactone (PCL) as the hydrophobic layers and carboxymethyl chitosan (CMC) and polyethylene oxide (PEO) as the hydrophilic layers, were fabricated by electrospinning. PCL is biocompatible, biodegradable, hydrophobic, and has good mechanical properties[,3]. CMC is water-soluble and has advantageous biological properties[4]. Micro-holes were made in meshes to improve cell infiltration. Then, multiple meshes were stacked together to create a mesh assembly with gradually decreasing pore sizes and densities from one side to the other. The top layer (opposite side from the wound) was comprised of non-punched fibrous meshes, which form a physical barrier for tissue penetration. This innovative design enables a faster cell-infiltration into the meshes, leading to a faster integration of the meshes and healing of the wound, while also enabling a progressive mechanical take-over from the meshes to newly regenerated tissue.

TABLE OF CONTENTS

LIST OF FIGURES

LIST OF TABLES

ACKNOWLEDGEMENTS

I would like to thank all those who have supported me throughout my academic career and time as a Schreyer Scholar. First, I would like to thank Dr. Jian Yang for his leadership over the past two and a half years as I have had had the privilege of learning from him and all of the dedicated and talented researchers in the Transformative Biomaterials and Biotechnology Laboratory. Second, I would like to express my immense gratitude to Dr. Zhiwei Xie, whose teaching guided me throughout the length of my project. Lastly, I would like to thank my family for their constant support as I have pursued my goals.

Chapter 1

Introduction

Hernia Repair Background

Hernia Incidence

A hernia is a defect on the abdominal wall with protrusion of other tissues, which occurs often clinically. Hernia repair is one of the most common surgeries in the world, with an estimated 20 million repairs performed each year[1]. With a lifetime risk of 27% for men and 3% for women in the United States and more than 990,000 abdominal wall hernias repaired every year, it is the second-most common surgical procedure in the country[2].

Hernia Diagnosis and Risk Factors

The abdominal wall is made up of layers: the skin, subcutaneous fascia, musculature, transversalis fascia, preperitoneal tissue, and peritoneum[5]. Abdominal hernias typically involve the inner four layers of the abdominal wall, connective tissue, and muscular fasciae[5]. Abdominal hernias can be diagnosed from a physical examination of a bulge that increases in size with coughing or straining. Patients usually report discomfort when lifting or straining. When there is strangulation of abdominal contents, patients experience severe pain and bowel obstruction can occur[2].

An abdominal hernia is classified as a protrusion through the abdominal wall that consists of intra-abdominal contents and with the sac lining intact[2]. This protrusion occurs when high intra-abdominal pressure affects the abdominal wall[2]. Typically, the increased intra-abdominal pressure is due

to prostatism, constipation, physical work, or chronic coughing[2]. In these patients, hernia repair is often successful when coupled with post-operative advice and decreased intra-abdominal pressure[2].

Risks Factors for Recurrence and Complications Following Hernia Repair

There are certain risk factors that can compromise the success of hernia repair. Wound infection is the most prominent risk factor for recurrence; thus, the majority of patients undergoing hernia repair receive antibiotics[6]. Additionally, some studies have found that larger hernias correspond to increased recurrences rates[6]. Further risk factors for recurrence include prostatism, abdominal aortic aneurysm surgery, suture repair, chronic constipation, chronic obstructive airways disease, smoking, and lifting[6]. These factors likely all increase the strain on the repair, leading to recurrence[6].

Major complications can arise after hernia repair. Recurrence is one of the most severe complications of hernia repair[7]. Patient activity or technical factors are accountable for early recurrences following hernia repair[2]. When there are late recurrences, aging factors or collagen build-up are typically responsible[2]. Chronic pain is another serious complication following hernia repair. Incidences of chronic pain have been found in various studies to range from 0 to 63% following hernia repair[7].

Hernia Mesh Repair

To treat abdominal hernias, the abdominal wall must be surgically repaired. Small hernias are repaired by simple sutures. However, suturing does not work on larger defects. Non-degradable fibrous meshes are currently the gold standard in the surgical treatment of hernias, having consistently lower recurrence rates than other techniques[6,7]. For mesh repair, the abdominal wall must be opened[2]. Once the hernial sac is pushed back into the abdominal cavity, a surgical mesh is applied[2]. Surgical meshes can be

placed intra-abdominally, on the surface of the peritoneal lining, or between layers of the abdominal wall[2].

However, even with mesh repair, there are still complications. In mesh repair, there is a recurrence rate of up to 10%. Further, 11% of patients suffer from chronic pain and 25% of these patients report moderate to severe pain[7]. Most patients describe the pain as neuropathic or aching[7]. Due to chronic pain, one-third of patients face limitations in their employment or daily leisure activities[7]. Additionally, intra-abdominal adhesions, erosion of intestines, and infection are major complications following mesh repair[2]. In general, infection is a common complication with implant materials[2]. In one-third of all implanted surgical meshes, bacterial colonization occurs, whether or not an infection is reported[2]. In hernia repair, the post-operative mesh infection incidence rate is 1-2%. These complications following hernia mesh repair indicated that there is a significant need for improvement in hernia repair techniques.

Hernia Mesh Materials

In hernia mesh repair, material selection is a vital element. It is necessary to consider both the mechanical properties of the mesh and the host response to material[2]. The human abdominal wall has a stiffness of 42.5 N in the transverse plane, 22.5 N in the sagittal plane, and a tensile strength of 16 N/cm[8]. In the epigrastric region, tissue ruptures at a horizontal load of 10.0 N/mm^2 and a vertical load of 4.5 N/mm^2 [9]. and Polypropylene (PP) mesh was first used for hernia repair by 1963; it was a breakthrough in terms of biocompatibility and comfort[2,6,10]. Currently, absorbable synthetic, non-absorbable synthetic, and organic meshes, including PP, polytetrafluoroethylene (PTFE), and nylon are available for use in hernia repair[2,6].

Non-Absorbable Meshes

The most common non-absorbable materials used today are PP and expanded polytetrafluroethylene (ePTFE)[6]. One consideration in material selection for hernia meshes is the potential for adhesion formation, as direct contact between intestines and synthetic materials can result in an inflammatory reaction[10]. PP is biocompatible and shows host tissue ingrowth, which can result in the formation of adhesions[2]. Thus, when it is in contact with intestines, adhesions can form and lead to complications[2]. Adhesions have also been reported with polyester meshes are used[2]. However, ePTFE has less host tissue ingrowth because it is hydrophobic; thus, it can be used intra-abdominally because it does not result in the formation of adhesions when in contact with intestines[2]. A second complication that must be considered when non-absorbable meshes are used is infection. PP meshes have infection rates ranging from 2.0-4.2%, ePTFE has infection rates ranging from 0-9.2% in open surgery and 0-1% in laparoscopic surgery, and polyester meshes have infection rates ranging from 7-16%[2]. Infection of meshes leads to more patient morbidity because of necessary follow-up operations, reduced wound healing, loss of function in the abdominal wall, and longer hospital stays[2]. A third consideration is the weight of the material, as light-weight and heavy-weight meshes have different effects when used[2]. Heavy-weight non-absorbable meshes result in an increased host tissue reactions, leading to increased collagen plate formation and more patient discomfort[2]. Additionally, heavy-weight meshes contract more upon application, leading to increased recurrence rates[2]. Thus, low-weight meshes are preferred in the use of non-absorbable meshes because they have increased abdominal wall compliance and result in less chronic pain [2]. However, low-weight meshes may not provide enough strength in the abdominal wall, leading to increased recurrence rates[2]. The material used in non-absorbable meshes has many implications in terms of complications following hernia mesh repair.

Absorbable Meshes

Absorbable meshes have been designed to battle the infection and patient morbidity risks of non-absorbable meshes[2,10]. Absorbable meshes are intended to support the abdominal wall upon repair, but then allow for the fibro-connective tissue to function as the main support once the mesh has been absorbed[2]. The meshes should become integrated into the abdominal wall without tension on the surrounding tissues[2]. Typically, absorbable meshes are synthesized from glycolic acid and lactic acid in varying ratios, resulting in varying degradation rates[2]. Absorbable meshes need to be optimized for use in hernia repair by designing them to have high biocompatibility, low adhesion formation, and low infection rates[2].

Cellular Meshes

Cellular meshes, or biological meshes, have also been explored. Risk factors of biological meshes that are not present in the use of synthetic meshes include immunologic rejection and transmission of disease[2]. However, cellular materials also have low infection rates[2]. Biological meshes, including those derived from human fascia lata, porcine small intestinal submucosa, acellular dermal matrix, and porcine dermal collagen have been used[2,10]. Unfortunately, these cellular meshes typically cost significantly more than polymeric meshes.

Electrospinning Fibrous Meshes

Electrospinning Process

Developing polymer meshes made from micro to nanometer-scale fibers via electrospinning has become a common and effective way to produce 3D scaffolds for tissue engineering. In electrospinning,

a polymer solution is pumped through a syringe with a metal tip[11]. A high voltage is applied to the needle tip, which causes the polymer solution drops to form in the shape of a cone[11]. The polymer solution is drawn to a grounding plate approximately 10 to 20 cm away[11]. As the polymer solution is drawn toward the grounding plate, the solvent evaporates and the fibers are collected on the plate[11]. Fibers in the range of nanometers to micrometers can be created[11]. The following diagram in Figure 1 shows a typical electrospinning setup.

-

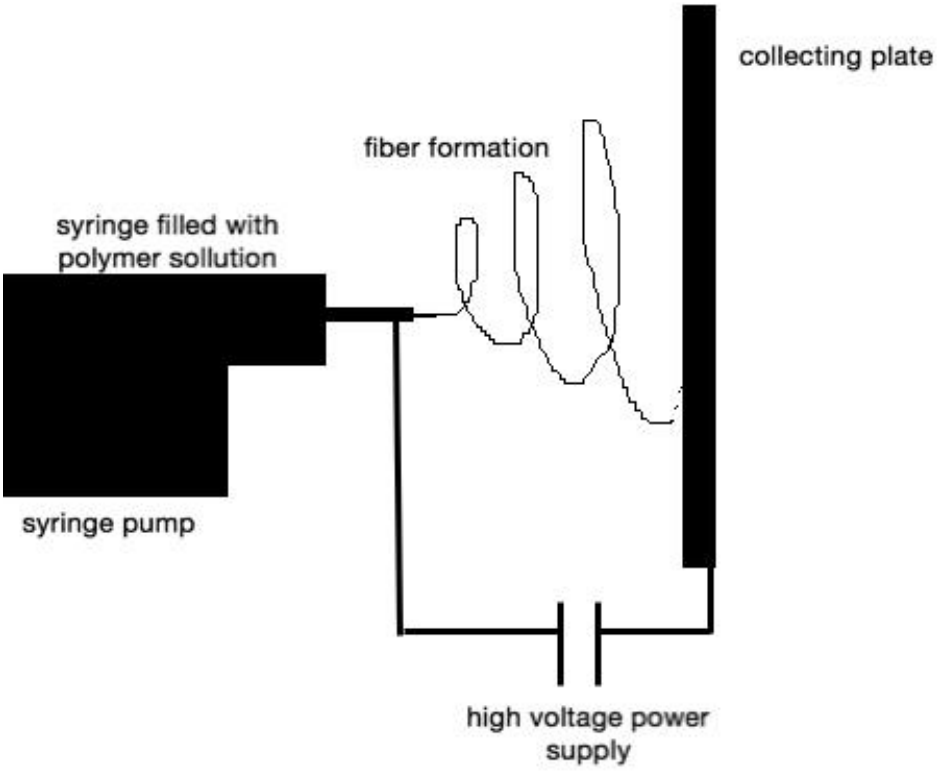

Figure 1: Illustration of a typical electrospinning setup

Common Electrospun Biomaterials

Many biopolymers have been electrospun[11]. In wound healing, chitin and chitosan are of special interest[11]. Chitosan/PVA blends have been found to have antibacterial properties[11]. Additionally, water-soluble polymers, such as PEO, PVA, poly(acrylic acid), polyacrylamide, polyelectrodes, polyvinylpyrrolidone, and hydroxypropylcellulose, are useful in biomedical applications because they decompose when in they come into contact with water[11].

Electrospinning Challenges

However, one of the major challenges of applying these electrospun fibers as tissue engineering scaffolds is poor cell infiltration into the 3D structure of the fibrous mesh[12]. Small pore sizes of electrospun meshed limit the cell infiltration from the surface to inside of the scaffold. Additionally, managing the mechanical performance of the mesh is a critical challenge of using electrospun meshes in tissue engineering applications such as hernia repair[7].

Our Strategy to Create Hernia Meshes

Project Goals

In this study, we developed an electrospun mesh that does not cause chronic pain or recurrence for hernia repair. The ideal mesh requires not only a soft nature and biodegradability, but also a gradual transfer of mechanical loads upon implantation to promote healing. Although existing biodegradable polymeric meshes hold promise in reducing chronic pain and potentially addressing other long-term concerns, their degradation rates hardly match new tissue formation and timely mechanical load transfer.

Step One

Thus, the first step of this project was to fabricate a novel biodegradable electrospun mesh with an elegant structural design to meet the mechanical requirements necessary for successful hernia repair by using a Design of Experiment study to optimize the electrospinning process.

Step Two

The second step of this project was to design the electrospun mesh to allow for faster cell infiltration and integration into the host tissue to improve the biological properties of meshes used in hernia repair.

Multi-Layered Micro-Patterned Electrospun Mesh Design

The following Figure 2 diagrams the design strategy for developing a multi-layered micro-patterned electrospun hernia mesh.

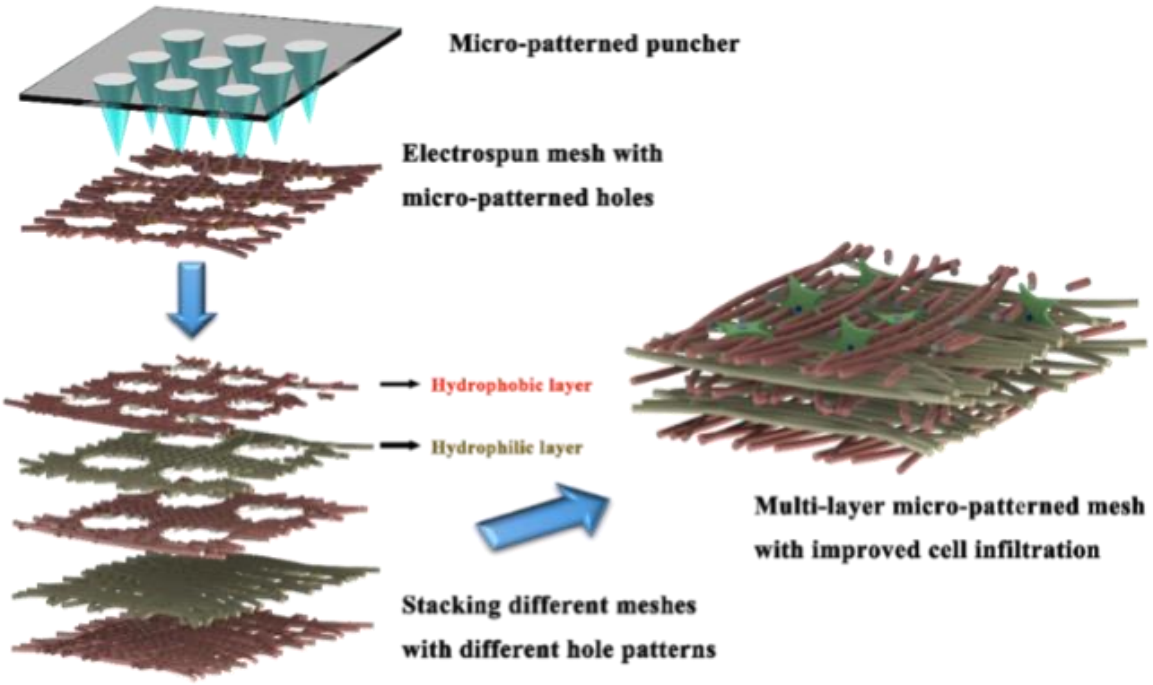

Figure 2: Illustration of fabricating and assembling multiple ES fibrous meshes with various densities of micro holes. Different sizes and densities of micro-holes can be patterned on both hydrophobic and hydrophilic meshes. The meshes with a gradient density of holes can be stacked into a hernia mesh that enables enhanced cell penetration into the 3D structure and a gradual mechanical force transfer upon tissue regeneration.

As illustrated in Figure 2, a novel design was developed for a multi-layered micro-patterned electrospun hernia mesh assembly that could also be used as a wound dressing. Biodegradable micro/nano-fibrous meshes, using polycaprolactone (PCL) as the hydrophobic layers and carboxymethyl chitosan (CMC) and polyethylene oxide (PEO) as the hydrophilic layers, were fabricated by electrospinning. PCL is biocompatible, biodegradable, hydrophobic, has good mechanical properties, and has been successfully electrospun before[13,3]. CMC is water-soluble and has advantageous biological properties[4]. CMC has also been successfully electrospun with PEO in water[4]. A custom-made hole punch was used to punch micro-holes on individual electrospun meshes. These micro-holes were designed to improve cell infiltration. Then, multiple meshes made of PCL or CMC/PEO were stacked together to create a mesh assembly with pores, which will allow cells to gradually penetrate throughout the mesh. This innovative design enables a faster cell-infiltration into the meshes, leading to a faster integration of

the meshes and healing of the wound, while also enabling a progressive mechanical take-over from the meshes to newly regenerated tissue.

Chapter 2

Methods

Electrospinning of PEO/CMC Mesh Layers

Solutions of carboxymethyl chitosan (CMC) (Santa Cruz Biotechnology, Dallas, TX) and poly(ethylene oxide) (PEO) (Sigma Aldrich, St. Louis, MO) were dissolved in DI water for electrospinning. PEO and CMC were dissolved in water and the solution was placed in a 1 mL syringe with a flat-tip needle. The syringe was secured to the syringe pump (PHD|Ultra, Harvard Apparatus, Holliston, MA). The voltage source (Gamma High Voltage Research, Ormond Beach, FL) was connected to the needle tip. A factorial analysis was used to determine the ideal electrospinning conditions. A metal grounding plate was placed 15 cm away from the needle tip of the syringe and an aluminum mesh was secured to the grounding plate to collect the fibers output from the syringe.

Electrospinning of PCL Mesh Layers

The ideal concentration of polycaprolactone (PCL) (Sigma Aldrich, St. Louis, MO) in chloroform was determined through experimental testing. Benzyltriethylammonium chloride salt (Sigma Aldrich, St. Louis, MO) was added to the PCL solutions to increase the conductivity of the solution. The same syringe, needle tip, and voltage source setup was used as in PEO/CMC electrospinning. Aluminum foil was secured to the grounding plate to collect the fibers. The ideal flow rate, 0.5 μl/min, and voltage, 24 kV, was determined through experimental testing.

Scanning Electron Microscopy

The fiber morphology and diameter of the PEO/CMC and PCL electrospun meshes were examined using scanning electron microscopy (SEM) (nanoSEM, FEI, Hillsboro, OR). The samples were coated with platinum using a sputter coater (Quorom EMS 150 Sputtter Coater) before imaging. Using ImageJ (National Institutes of Health, Bethesda, MD, USA), the SEM images were analyzed. The average fiber diameters were determined for each mesh by randomly selecting 20 fibers from 4 images taken of a given mesh (for a total of 80 measurements per mesh) and averaging the results.

Factorial analysis

A two-level factorial design was used to determine the ideal electrospinning conditions for of the PEO/CMC meshes. Design-Expert®, a design-of-experiments (DOE) software (State-Ease, Inc., Minneapolis, MN), was used to perform the full-factorial two-level design study. CMC concentration, PEO concentration, voltage, and the presence of salt (NaCl) were chosen as key factors to evaluate. For each key factor, realistic high and low values were chosen based on exploratory experiments and input into Design-Ease. Table 1 shows the key factors studied.

Table 1: Key factors studied in the factorial analysis

	Low	High
CMC concentration (g/ml)	3	5
PEO concentration (g/ml)	5	8
Voltage (kV)	16	24
Salt (used or not used)	0	1

Design-Ease then outlined the formulations of electrospinning in random order that were tested, as shown in Table 2.

Table 2: Formulations studied in the factorial analysis

Factor 1: CMC concentration (g/ml)	Factor 2: PEO concentration (g/ml)	Factor 3: Voltage (kV)	Factor 4: Salt (present or not)
5	8	16	1
3	5	24	0
3	8	24	1
5	8	24	0
5	5	24	0
3	5	24	1
3	8	16	1
5	5	16	1
3	5	16	0
3	8	24	0
3	8	16	0
5	8	24	1
5	5	16	0
5	5	24	1
3	5	16	1
5	8	16	0

Fiber diameter and standard deviation of the fiber diameter were chosen as response factors. Fiber diameters of the meshes were determined, as previously described, from SEM images using ImageJ analysis. The software provided outputs in the form of half-normal probability plots and surface diagrams.

Mechanical Testing

Tensile mechanical testing was performed using a mechanical tester (model 5966, Instron, Norwood, MA). Meshes were cut into rectangular samples with dimensions of 25 mm X 7 mm X 0.5 mm. The samples were elongated to failure at a rate of 500 mm/min using a 500 N load cell. Stress-strain curves were obtained and the tensile strength, elongation at break, and initial modulus were determined for the meshes.

Cell Proliferation Studies

Cell proliferation studies were performed on PCL, PEO/CMC, and multi-layered meshes. Samples of each mesh type were fit to a transparent, flat-bottomed 96 well plate (Corning, NY). The samples were sterilized under ultraviolet light. Mouse 3T3 fibroblast cells were seeded into the wells at 2,000 cells/well in 200 µl of Dulbecco's Modified Eagle Medium (DMEM supplemented with 10% FBS and 1% Penicillin Streptomycin) and incubated at 37 C with 5% CO2 and 95% humidity for one week. After 3 days, a CCK-8 assay was used to determine the cell proliferation on the samples.

Preparation of a Multi-Layered Micro-Patterned Electrospun Mesh

The PCL and PEO/CMC meshes bound together using injectable citrate-based mussel-inspired bioadhesive (iCMBA). Uniform holes were punched through the PCL layers using a custom-made punch with an array of microneedles. The diameter of the holes created was 483 µm and holes were spaced 1.5 mm apart, which was measured by SEM images. The custom punch is shown in Figure 3.

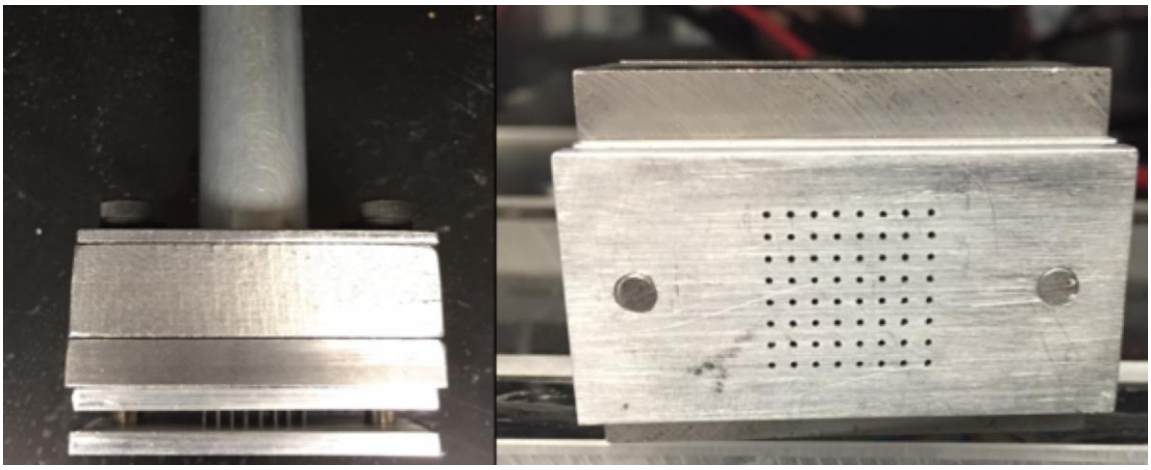

Figure 3: Custom-made hole punch

Chapter 3

Results

Electrospun Fiber Morphology and Structures

First, the fiber morphology and structures with different electrospinning conditions were visualized by SEM. The SEM images of the PEO/CMC meshes electrospun for the factorial analysis were analyzed in ImageJ. Sample images at each condition are shown below. Figures 4(a-d) show 5% PEO 3% CMC meshes at the various electrospinning conditions.

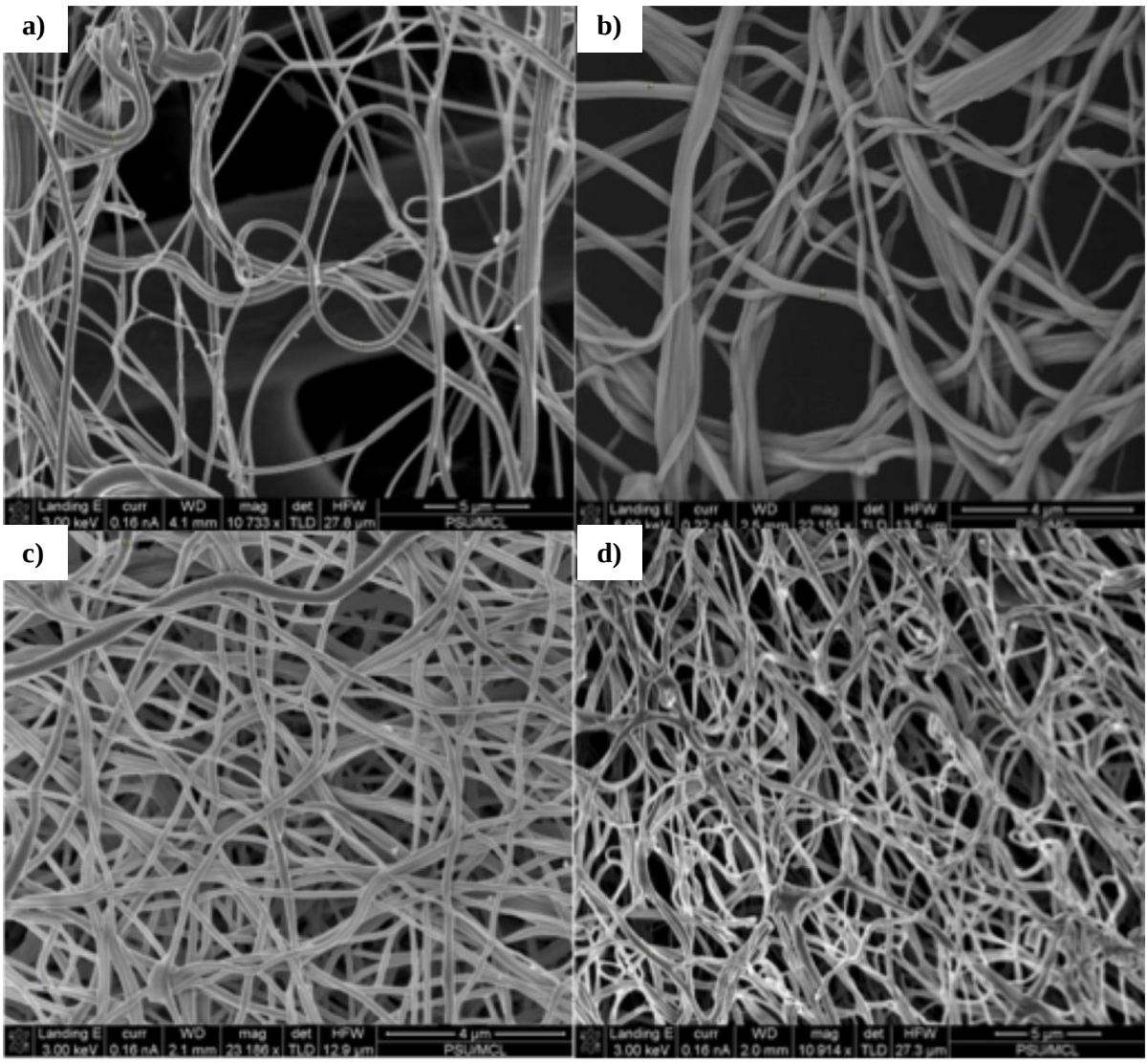

Figure 4a: SEM images of 5% PEO, 3% CMC, no salt, 16 kV; Figure 4b: 5% PEO, 3% CMC, salt, 16 kV; Figure 4c: 5% PEO, 3% CMC, no salt, 24 kV; Figure 4d: 5% PEO, 3% CMC, salt, 24 kV

Figures 5(a-d) show 5% PEO 5% CMC meshes at the various electrospinning conditions.

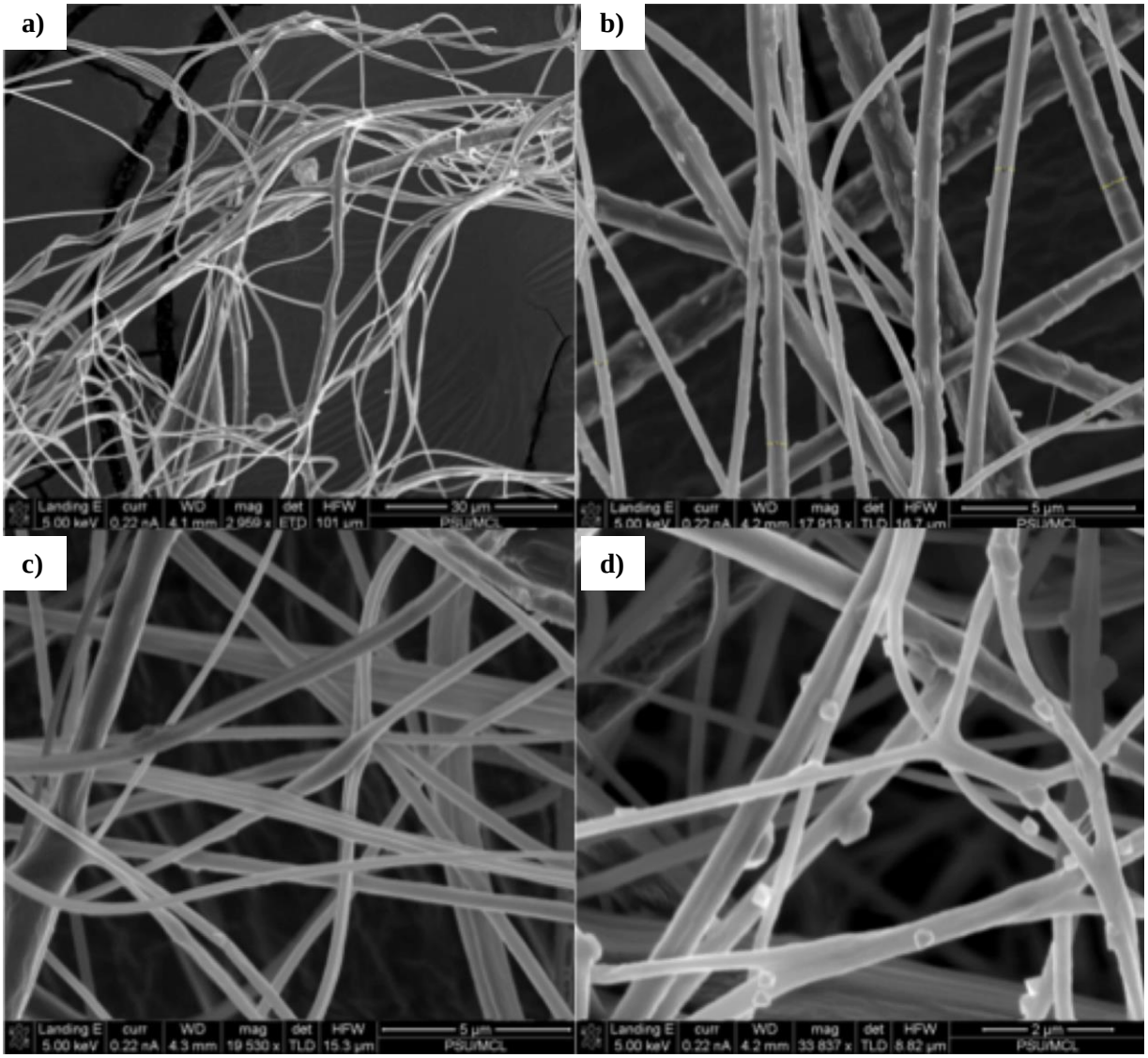

Figure 5a: 5% PEO, 5% CMC, no salt, 16 kV; Figure 5b: 5% PEO, 5% CMC, salt, 16 kV; Figure 5c: 5% PEO, 5% CMC, no salt, 24 kV; Figure 5c: 5% PEO, 5% CMC, salt, 24 kV

Figures 6(a-d) show 8% PEO 3% CMC meshes at the various electrospinning conditions.

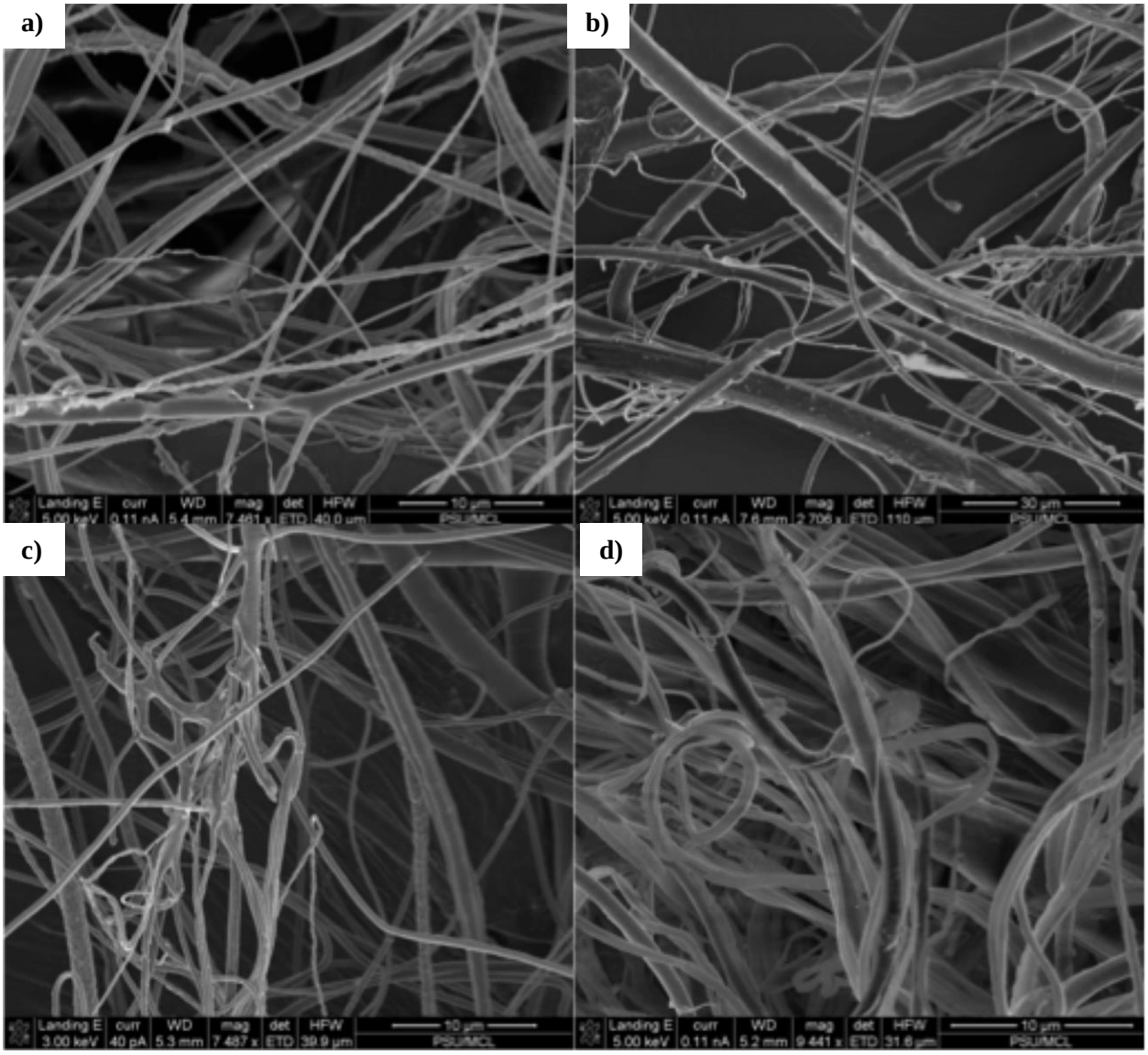

Figure 6a: 8% PEO, 3% CMC, salt, 16 kV; Figure 6b: 8% PEO, 3% CMC, no salt, 16 kV; Figure 6c: 8% PEO, 3% CMC, no salt, 24 kV; Figure 6d: 8% PEO, 3% CMC, salt, 24 kV

The average fiber diameters and standard deviations were calculated for each condition from the ImageJ analysis, as shown in Table 3.

Table 3: The fiber diameters and standard deviations of fiber diameter at all of the conditions tested in the factorial analysis

	5% PEO, 3% CMC, no salt,16 kV	**5% PEO, 3% CMC, salt, 16 kV**	**5% PEO, 3% CMC, no salt, 24 kV**	**5% PEO, 3% CMC, salt, 23 kV**
Average Fiber Diameter (µm)	0.29 ± 0.14	0.29 ± 0.17	0.15 ± 0.05	0.23 ± 0.12
	5% PEO, 5% CMC, no salt, 16 kV	**5% PEO, 5% CMC, salt, 16**	**5% PEO, 5% CMC, no salt, 24 kV**	**5% PEO, 5% CMC, salt, 24 kV**
Average Fiber Diameter (µm)	0.73 ± 0.53	0.52 ± 0.30	0.50 ± 0.27	0.53 ± 0.29
	8%, 3% CMC, no salt, 16 kV	**8% PEO, 3% CMC, salt, 16 kV**	**8% PEO, 3% CMC, no salt, 24 kV**	**8% PEO, 3% CMC, salt, 24 kV**
Average Fiber Diameter (µm)	0.84 ± 0.57	2.07 ± 3.12	0.71 ± 0.60	0.78 ± 0.52

Factorial Analysis

To optimize the electrospinning conditions for CMC/PEO fibers, a 2k factorial analysis was performed. In Figure 6, the interaction of voltage, CMC concentration, and salt content its effect on the fiber diameter is shown. Each edge of the cube represents a factor and its high to low values and the back face shows the fiber diameter. Each corner shows the fiber diameter at the corresponding factor values. It can be seen that the smallest fiber diameter occurs at no salt content, low CMC concentration, and high voltage.

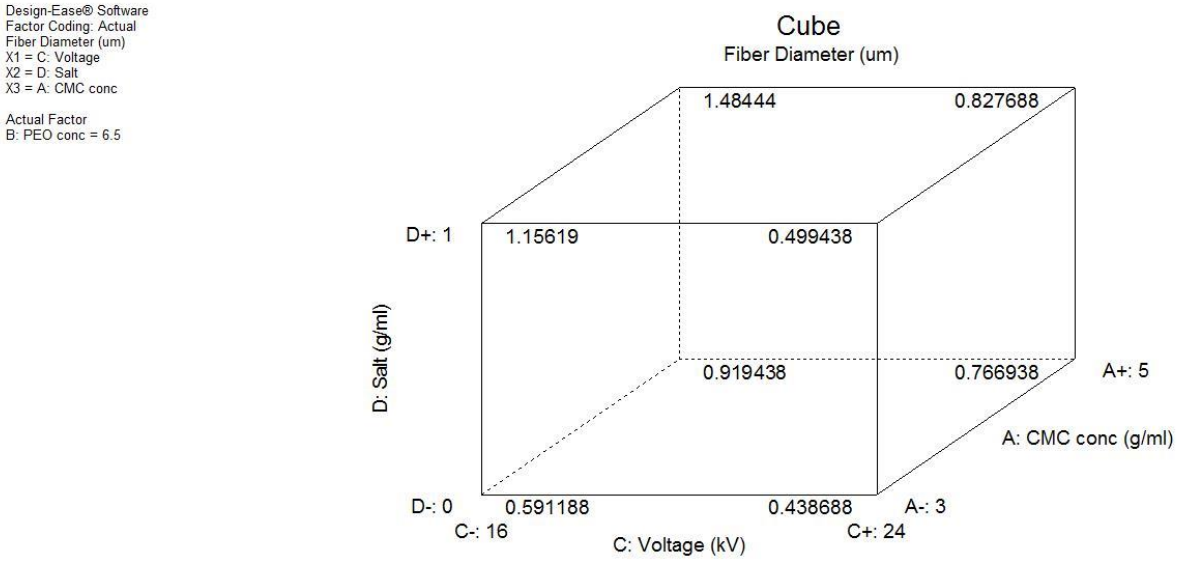

Figure 6: The interaction of voltage, CMC concentration, and salt content and the effect on fiber diameter

In Figure 7, the interaction of voltage, PEO concentration, and CMC concentration and the effect on fiber diameter is shown. The smallest fiber diameter occurs at high voltage and low PEO concentration.

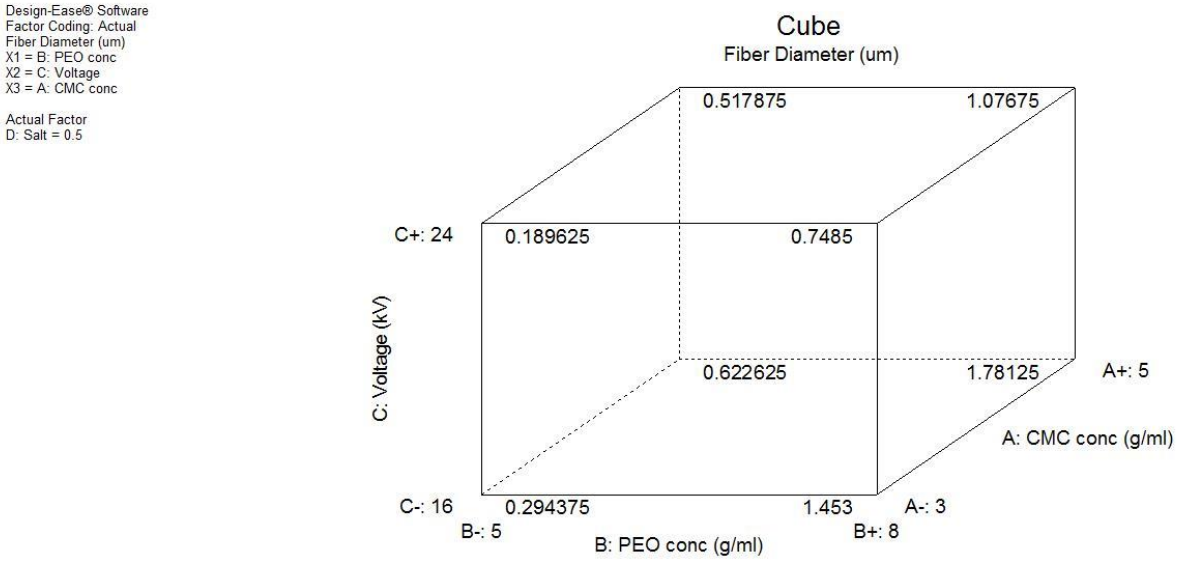

Figure 7: The interaction of voltage, PEO concentration, and CMC concentration and the effect on fiber diameter

In Figure 8, the interaction of PEO concentration and CMC concentration and the effect on fiber diameter is shown. This figure also shows that the smallest fiber diameter occurs at low PEO concentration and low CMC concentration, with PEO concentration having a larger effect on fiber diameter.

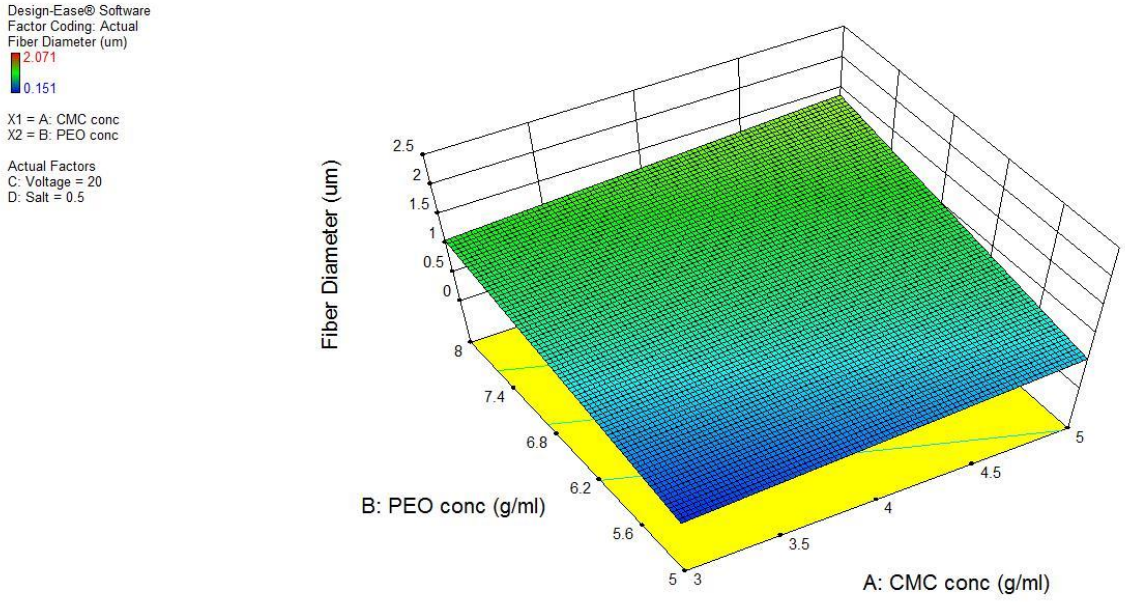

Figure 8: A surface diagram to show the interaction of PEO and CMC concentration

In Figure 9, the interaction of voltage and PEO concentration and the effect on fiber diameter is shown. It can be seen that the smallest fiber diameter occurs at high voltage and low PEO concentration. Additionally, PEO concentration has a larger effect on fiber diameter than does the voltage.

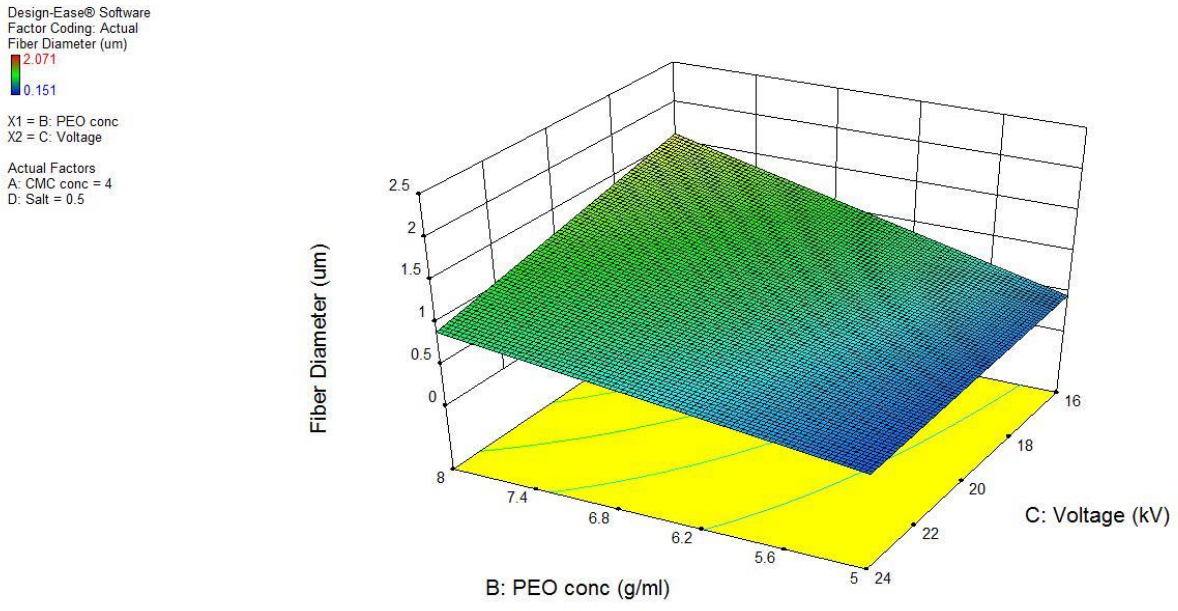

Figure 9: A surface diagram to show the interaction of voltage and PEO concentration and the effect on fiber diameter

In Figure 10, the interaction of PEO concentration and salt and the effect on fiber diameter is shown. From the figure, it can be seen that PEO concentration has a larger effect on fiber diameter than does salt content, with the smallest fiber diameter occurring at zero salt content and low PEO concentration.

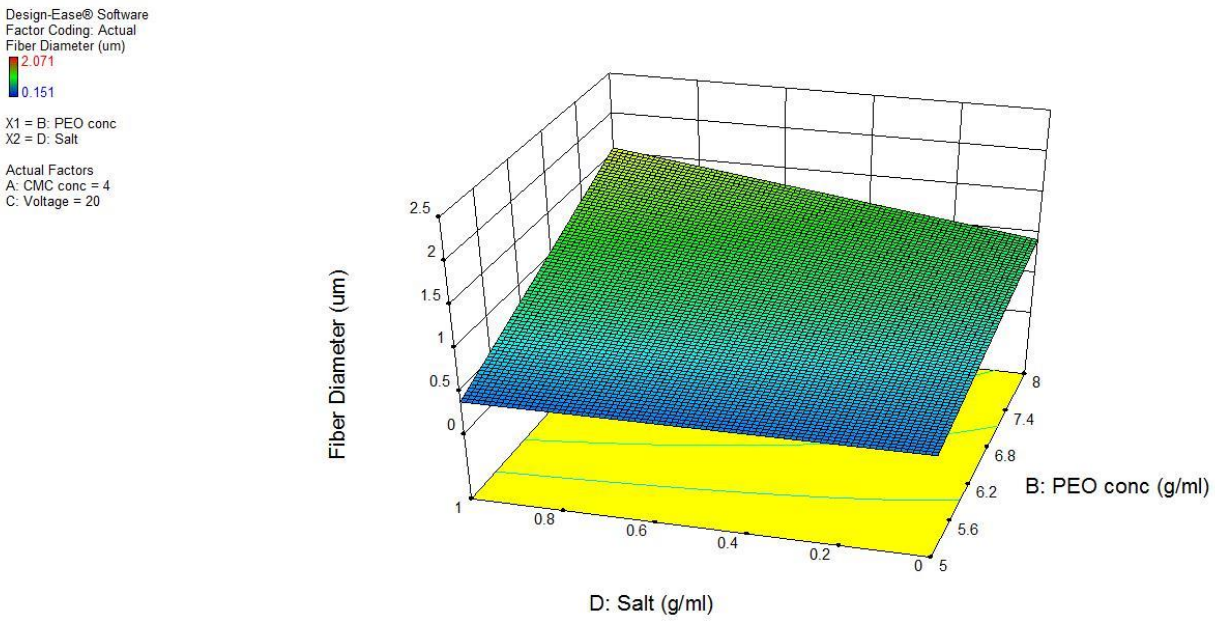

Figure 10: A surface diagram to show the interaction of salt and PEO concentration and the effect on fiber diameter

In Figure 11, the interaction of salt content and voltage and the effect on fiber diameter is shown. It can be seen that the salt content affects the fiber diameter more than the voltage does.

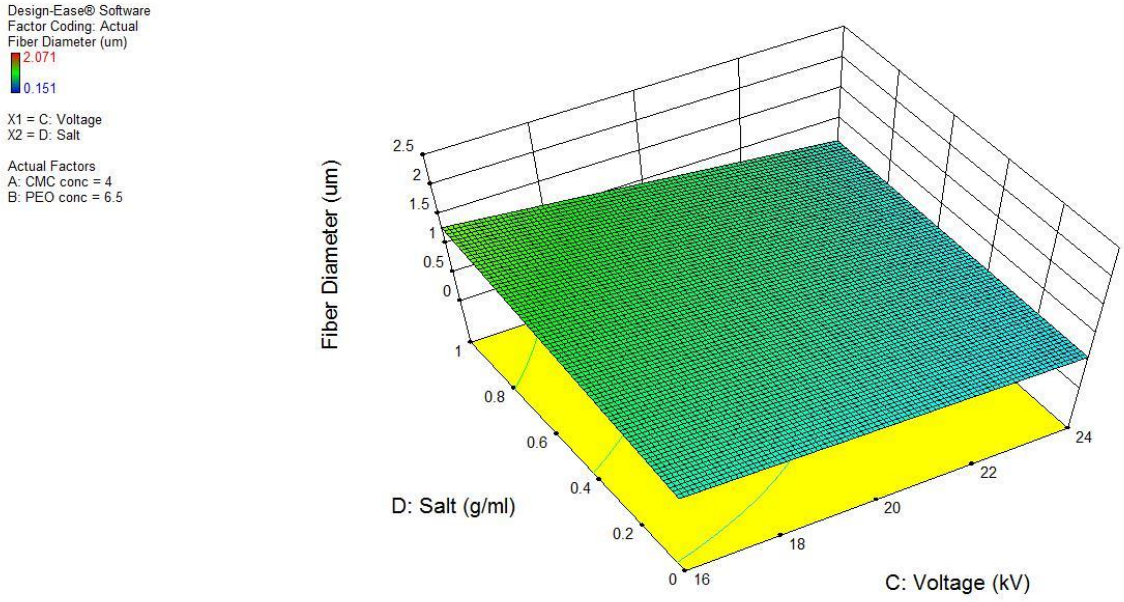

Figure 11: A surface diagram to show the interaction of salt content and voltage and the effect on fiber diameter

In Figure 12, the interaction of voltage, PEO concentration, and CMC concentration and the effect on the standard deviation of fiber diameter is shown. As seen in this figure, the smallest standard deviation in fiber diameter occurs at low PEO concentration, low CMC concentration, and high voltage.

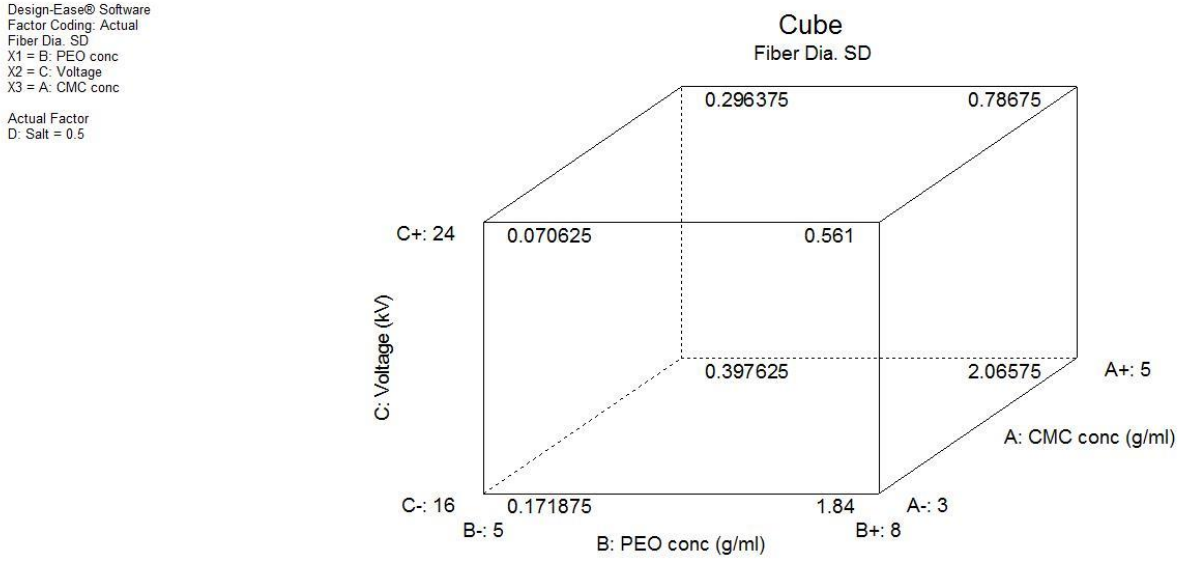

Figure 12: The interaction of voltage, CMC concentration, and PEO concentration and the effect on the standard deviation of the fiber diameter

In Figure 13, the interaction of CMC concentration and PEO concentration and the effect on the standard deviation of fiber diameter is shown. The smallest standard deviation occurs at low CMC concentration and low PEO concentration. Additionally, PEO concentration has a larger effect on the standard deviation of the fiber diameter than does CMC concentration.

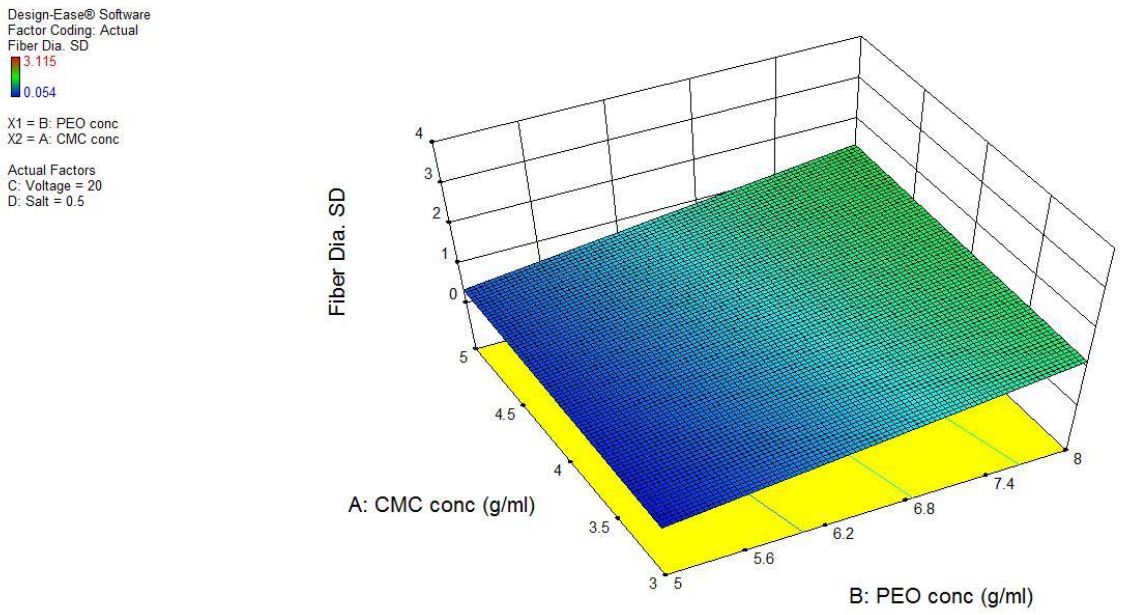

Figure 13: A surface diagram to show the interaction of CMC concentration and PEO concentration and the effect on the standard deviation of fiber diameter

In Figure 14, the interaction of voltage and PEO concentration and the effect on the standard deviation of the fiber diameter is shown. The smallest standard deviation occurs at high voltage and low PEO concentration. Additionally, PEO concentration has a greater effect on the standard deviation of fiber diameter than does voltage.

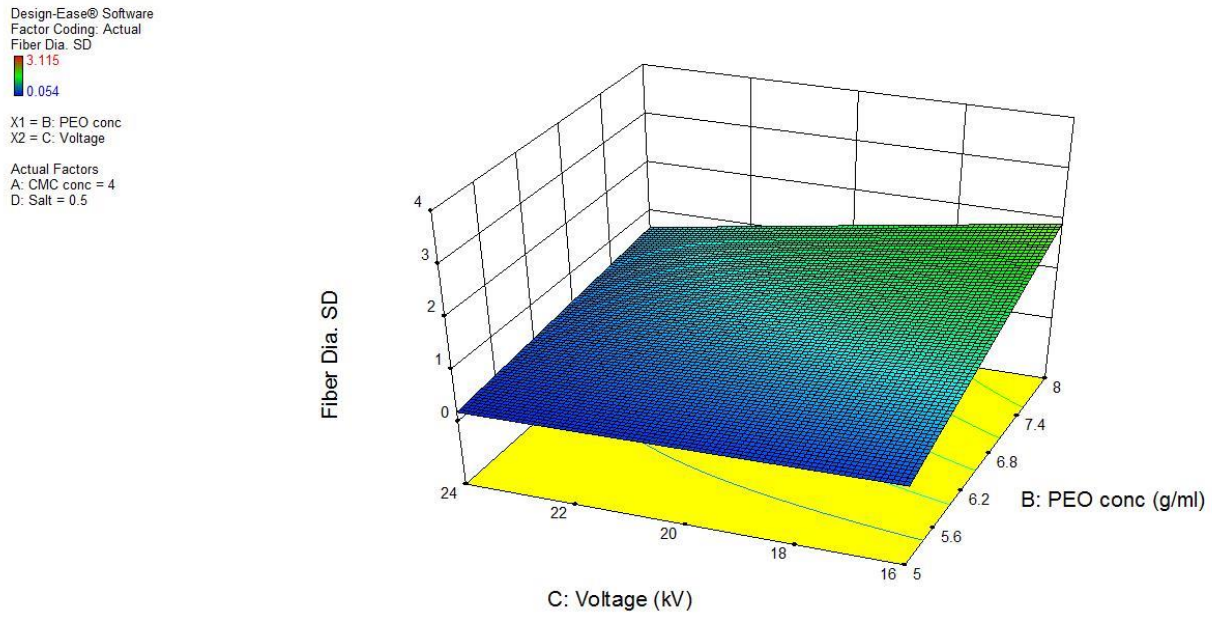

Figure 14: A surface diagram to show the interaction of voltage and PEO concentration and the effect on the standard deviation of the fiber diameter

In Figure 15, the interaction of salt content and PEO concentration and the effect on the standard deviation of the fiber diameter is shown. The smallest standard deviation occurs at zero salt content and low PEO concentration. Additionally, PEO concentration has a larger effect on the standard deviation of the fiber diameter than does the salt content.

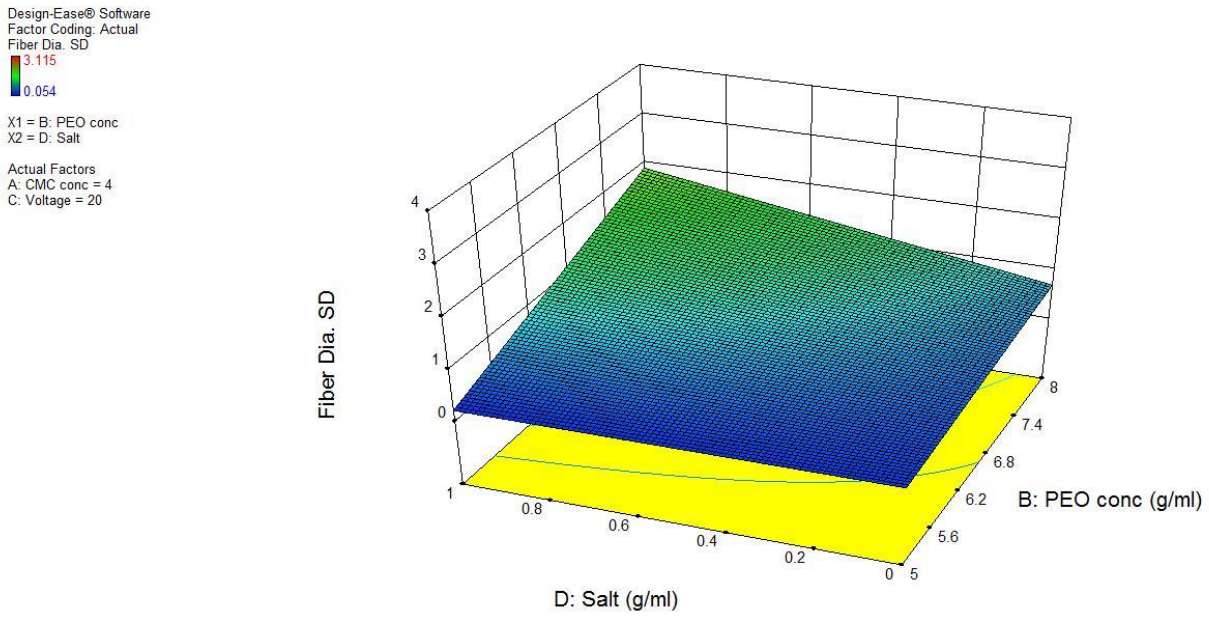

Figure 15: A surface diagram to show the interaction of salt and PEO concentration and the effect on the standard deviation of fiber diameter

In Figure 16, the interaction of CMC concentration and salt content and the effect on the standard deviation of fiber diameter is shown. It can be seen that the smallest standard deviation in fiber diameter occurs at low CMC concentration and zero salt content. Additionally, the salt content has a larger effect on the standard deviation than does the CMC concentration.

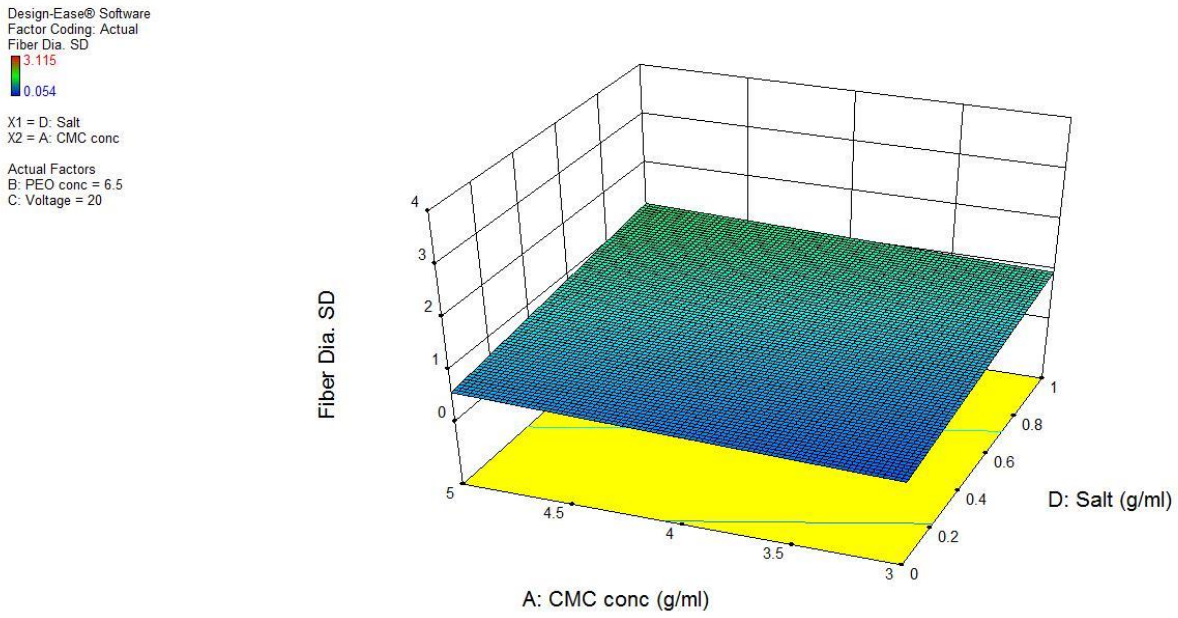

Figure 16: A surface diagram to show the interaction of CMC concentration and salt content and the effect on the standard deviation of the fiber diameter is shown

Additionally, equations were output from the factorial analysis. Equation in terms of actual factors can be used to make predictions about the response for given levels of each factor. The levels are in terms of the original units for each factor. In Figure 17, the equation for the fiber diameter in terms of the actual factors is shown.

Fiber Diameter =

-0.37971
+0.16412 * CMC conc
+0.12054 * PEO conc
-0.036125 * Voltage
-7.07800 * Salt
+2.62500E-003 * PEO conc * Voltage
+1.33100 * PEO conc * Salt
+0.29596 * Voltage * Salt
-0.055229 * PEO conc * Voltage * Salt

Figure 17: Fiber diameter equation in terms of actual factors

Additionally, equations can be given in terms of coded factors. These equation can be used to make predictions about the response for given levels of each factor. Coded equations can be used to identify the relative impact of factors by comparing the factor coefficients. In Figure 18, the coded equation for fiber diameter is given where A is CMC concentration, B is PEO concentration, C is voltage, and D is salt.

Fiber Diameter =

+0.84

+0.16 * A

+0.43 * B

-0.20 * C

+0.16 * D

-0.15 * BC

+0.17 * BD

-0.13 * CD

-0.17 * BCD

Figure 18: Fiber diameter equation in terms of coded variables

From the fiber diameter coded factor equation, it can be determined that PEO concentration has the largest effect on fiber diameter, followed by voltage, and then CMC concentration and salt content having equal effects.

In Figure 19, the equation for the standard deviation of fiber diameter in terms of the actual factors is given.

Fiber Dia. SD =

+0.36404

+0.11288 * CMC conc

-0.026208 * PEO conc

-0.065667 * Voltage

-14.06867 * Salt

+8.77083E-003 * PEO conc * Voltage

+2.73483 * PEO conc * Salt

+0.59675 * Voltage * Salt

-0.11569 * PEO conc * Voltage * Salt

Figure 19: Standard deviation of fiber diameter equation in terms of actual factors

In Figure 20, the equation for standard deviation of the fiber diameter in terms coded factors is given where A is CMC concentration, B is PEO concentration, C is voltage, and D is salt.

Fiber Dia. SD =

+0.77

+0.11 * A

+0.54 * B

-0.35 * C

+0.30 * D

-0.29 * BC

+0.32 * BD

-0.31 * CD

-0.35 * BCD

Figure 20: Equation for the standard deviation of fiber diameter in terms of coded factors

From the coded factor equation for standard deviation of diameter, it can be seen that PEO concentration has the largest effect on fiber diameter followed by voltage, salt content, and then CMC concentration.

Overall, from the factorial analysis, it was determined that the smallest fiber diameter occurs at low PEO concentration, low CMC concentration, zero salt content, and high voltage. Further, the smallest standard deviation in fiber diameter occurs at low PEO concentration, low CMC concentration, zero salt content, and high voltage. Thus, these conditions were determined to be ideal for electrospinning PEO/CMC meshes.

Micro-Hole Fabrication

Micro-holes were created in the meshes using a custom-made punch. CMC/PEO meshes with holes are shown in Figures 21(a-d). Clean edges can be observed after cutting. The average pore size is 483 µm. The average pitch between each hole is 1.5 mm.

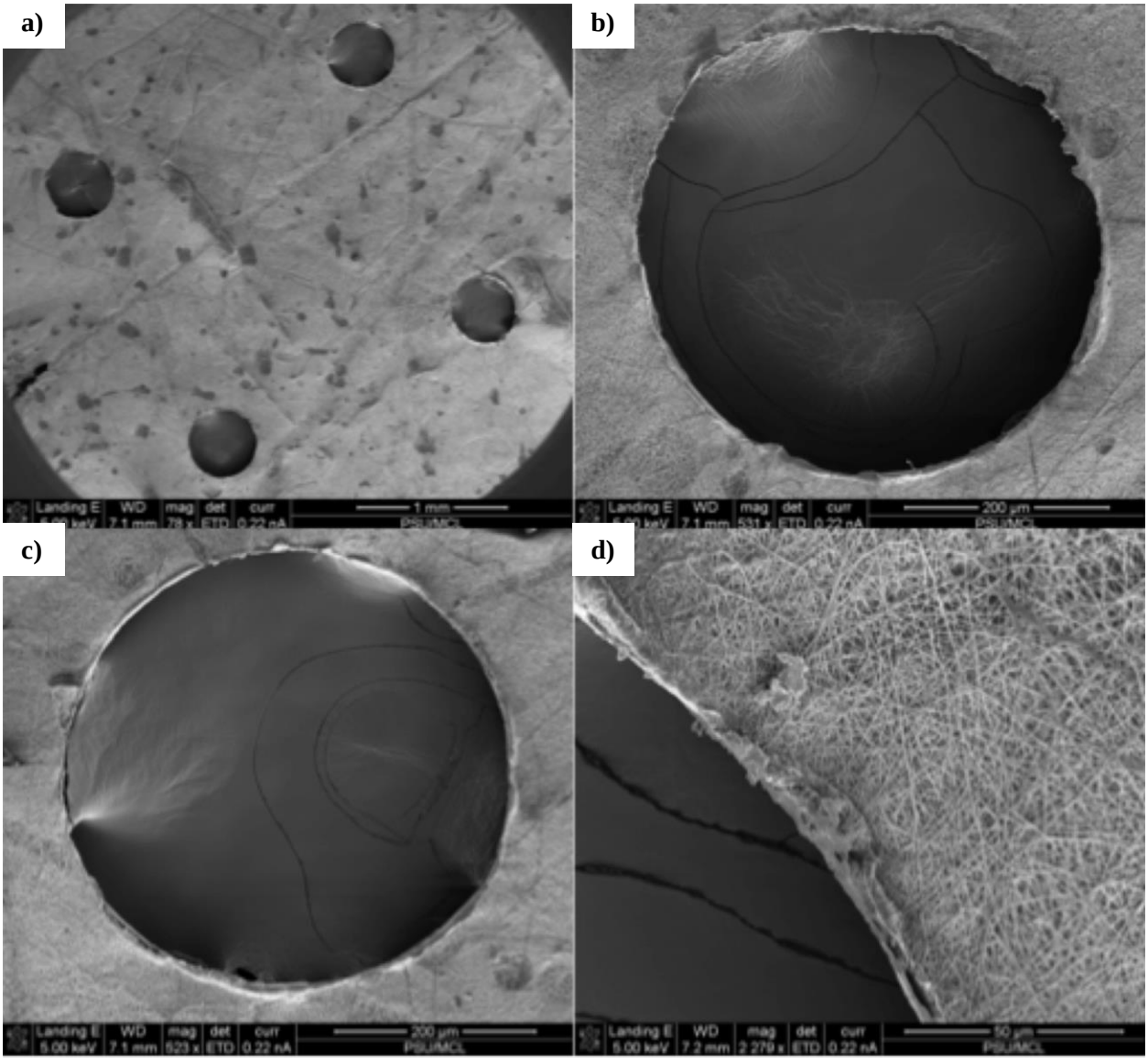

Figure 21(a-d): CMC/PEO meshes with holes made with the custom punch

In Figures 22(a-b), PCL meshes with holes made using the custom-made punch are shown. The edges are not as clean as the CMC/PEO meshes, probably because that PCL is much more elastic. Again, the average pore size is 483 μm. The average pitch between each hole is 1.5 mm.

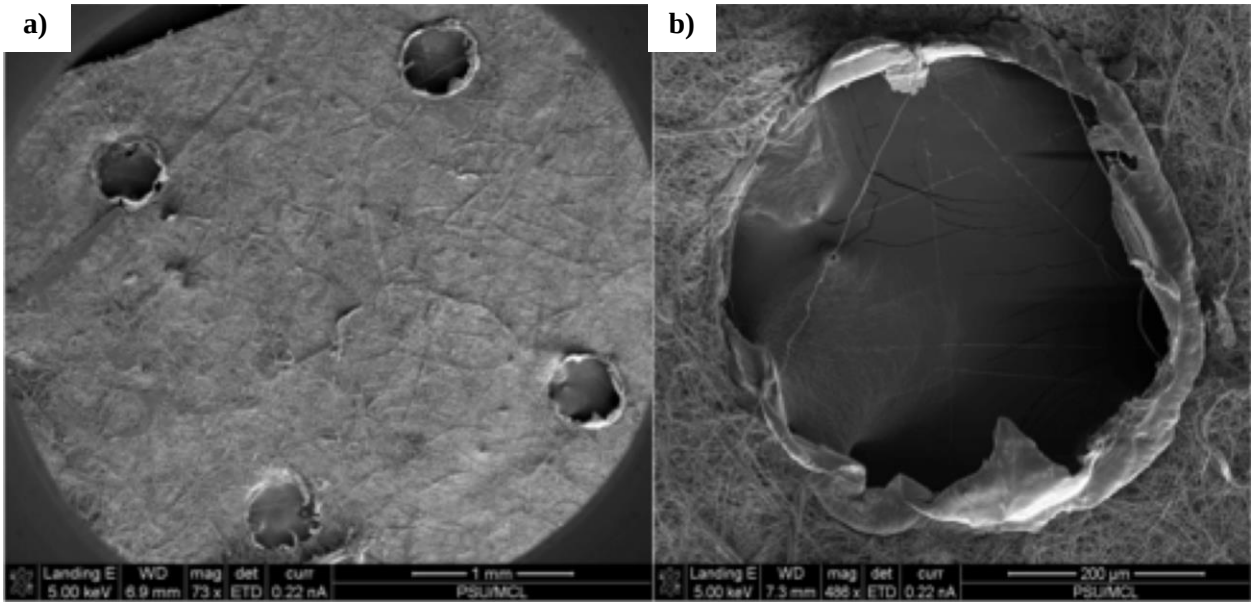

Figure 22(a-b): PCL meshes with holes

Binding the Layers

To create a multiple-layer electrospun mesh composite, the PCL layers were bound to the CMC/PEO layers by spraying the PCL with iCMBA, which is an adhesive polymer developed in our lab previously[14], with periodate as the catalyst and then electrospinning CMC/PEO layers on top of the PCL layers. Figures 23(a-b) show the binding of the layers with iCMBA. In the figures, PCL is bound between two layers of CMC/PEO.

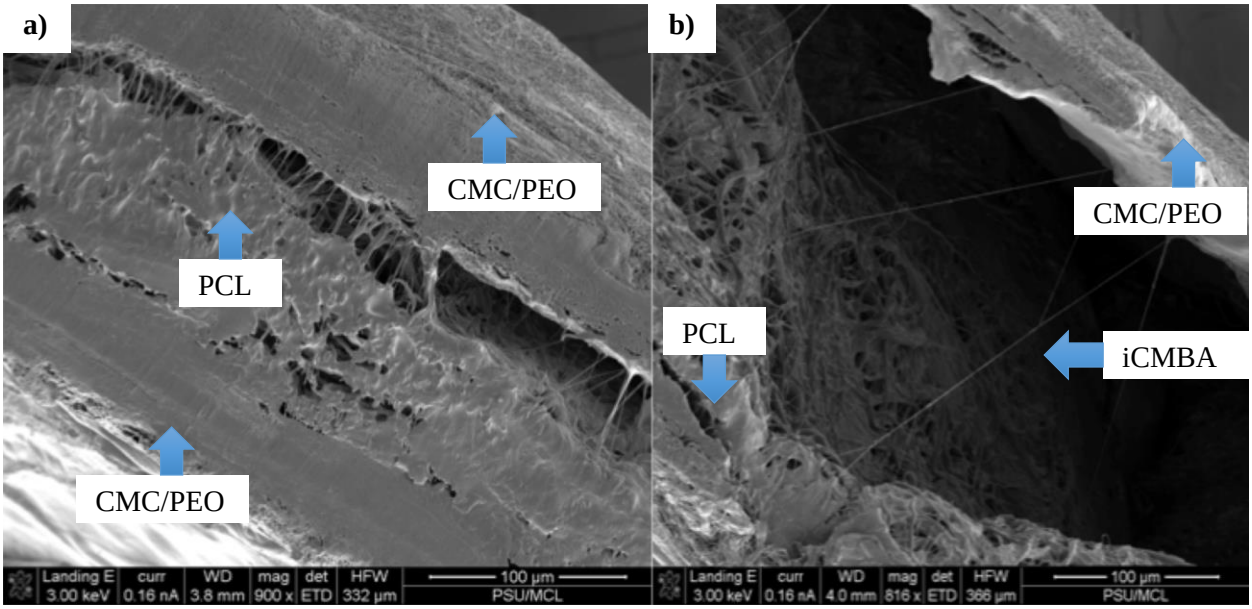

Figure 23(a-b): PCL bound in-between two layers CMC/PEO connected with iCMBA

Mechanical Properties

Next, the mechanical performance was evaluated by a tensile mechanical test. PCL meshes, PCL meshes with cells seeded, and PCL meshes with holes were tested. CMC/PEO meshes with and without holes were tested. After combining the different layers together, the tensile performance was investigated again using a 4-layer mesh as an example, (2 CMC/PEO and 2 PCL), both with and without holes. From the stress-strain curves of the meshes, the peak stress, initial modulus, elongation at break, and peak load were obtained, as shown in Figures 24, 25, 26, and 27.

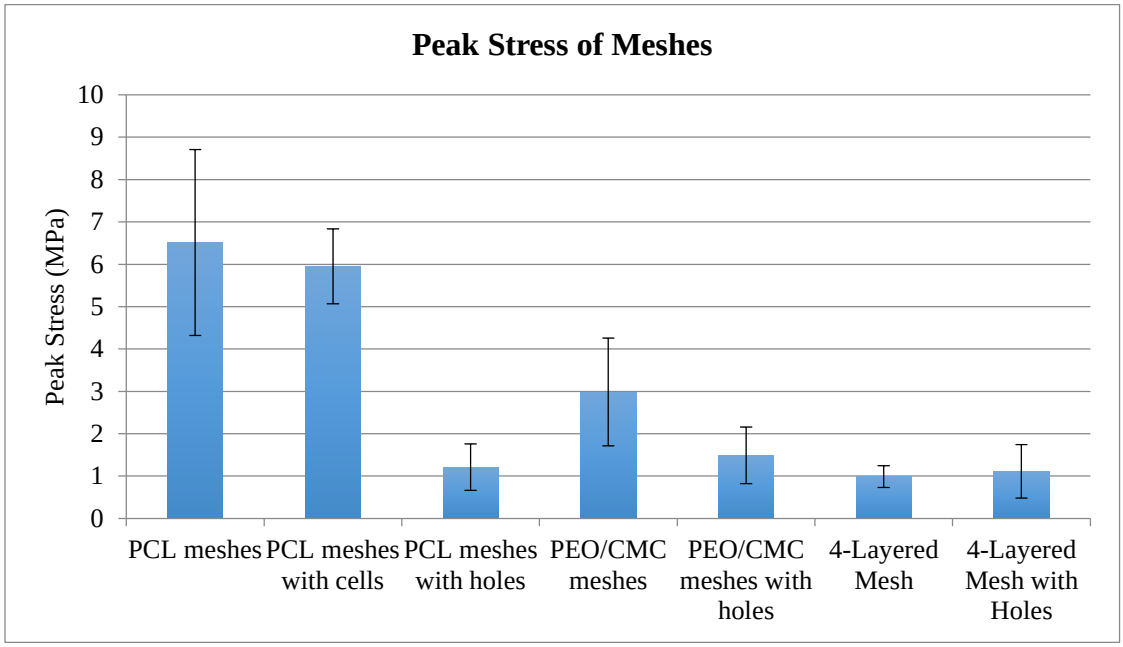

Figure 24: Peak stress of the meshes

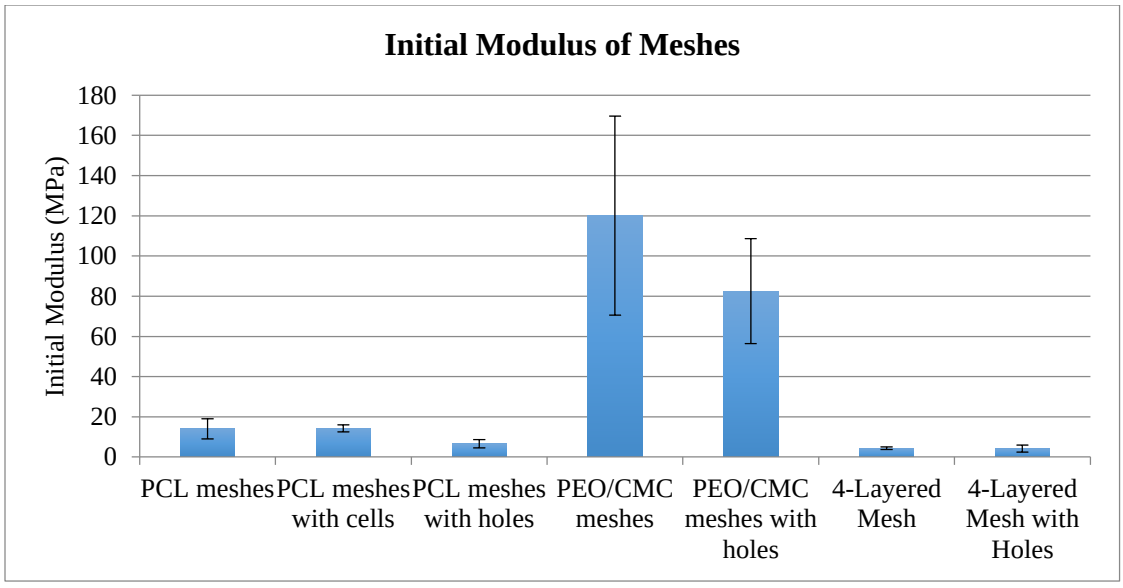

Figure 25: Initial modulus of meshes

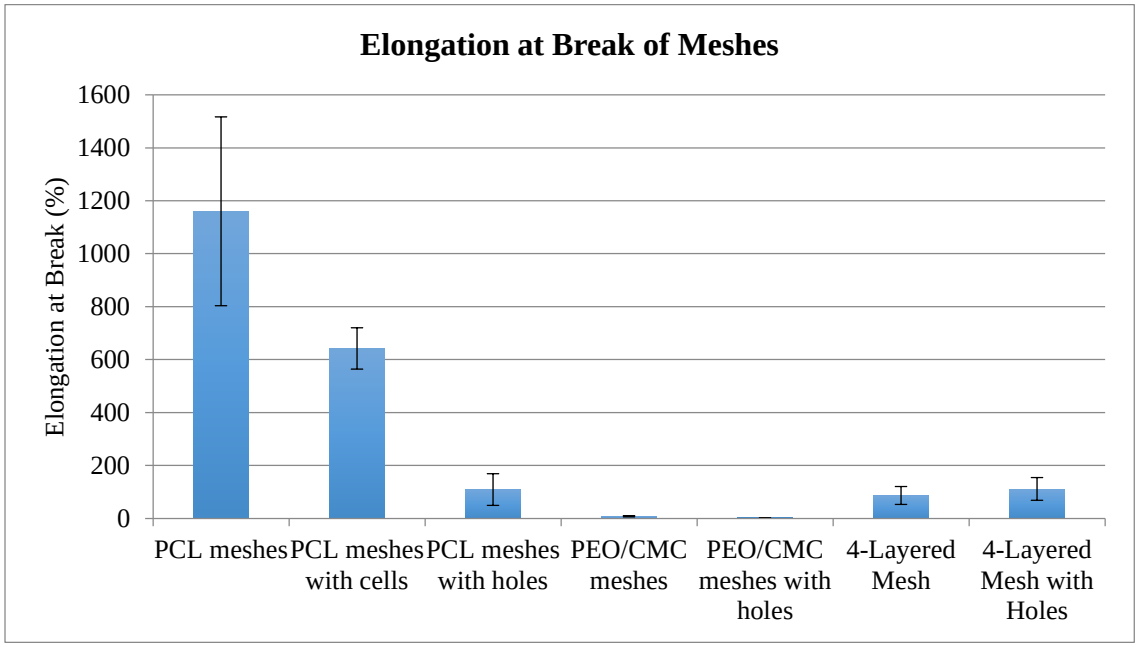

Figure 26: Elongation at break of meshes

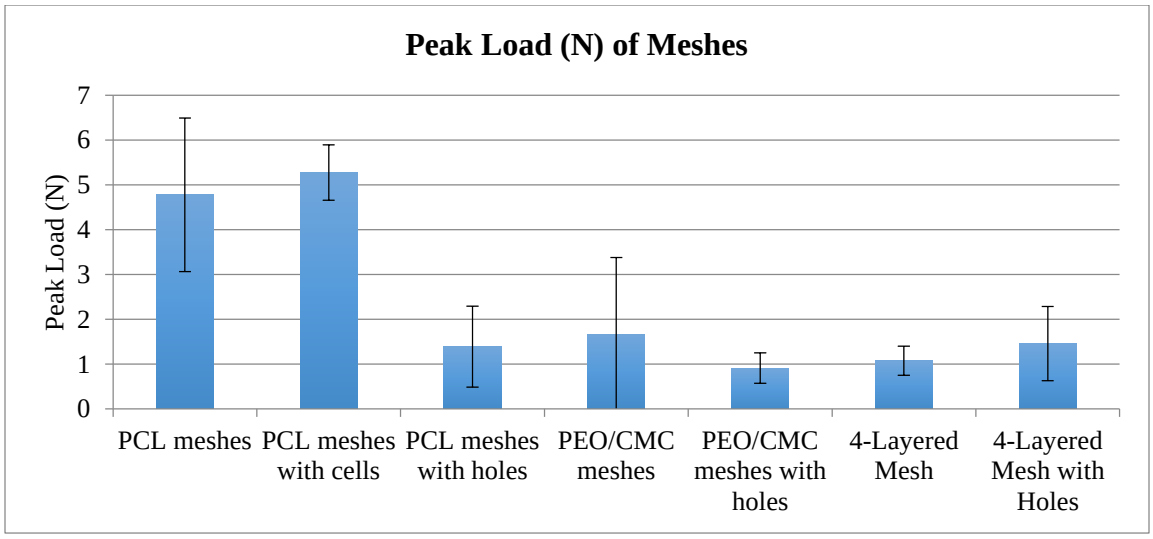

Figure 27: Peak load of meshes

The compiled peak stress, breaking elongation, initial modulus, and peak load from the tensile mechanical testing of meshes are summarized in Table 4. It is clear that with holes on the mesh, the peak stress and elongation at break decreased dramatically, while the initial modulus also decreased. Interestingly, the cell seeded PCL mesh exhibited moderately decrement in all considerations. It is also noticed that the 4-layer meshes were not as strong as CMC/PEO or PCL meshes alone, probably due to

the weak interface interactions. The combined mesh also showed softer and more elastic performance than the CMC/PEO itself.

Table 4: Mechanical Testing Data

	Peak Stress (MPa)	Initial Modulus (MPa)	Elongation at Break (%)	Peak Load (N)
PCL meshes	6.5 ± 2.2	14.1 ± 5.0	1,160.1 ± 357.0	4.8 ± 1.7
PCL meshes with cells	6.0 ± 0.9	14.2 ± 1.8	641.8 ± 78.1	5.3 ± 0.6
PCL meshes with holes	1.2 ± 0.5	6.6 ± 2.1	109.2 ± 59.9	1.4 ± 0.9
PEO/CMC meshes	3.0 ± 1.3	120.1 ± 49.5	7.7 ± 2.5	1.7 ± 1.7
PEO/CMC meshes with holes	1.5 ± 0.7	82.5 ± 26.2	2.2 ± 0.4	0.9 ± 0.4
4-Layered Mesh	1.0 ± 0.3	4.4 ± 0.6	87.2 ± 33.9	1.1 ± 0.3
4-Layered Mesh with Holes	1.1 ± 0.6	4.2 ± 1.8	111.4 ± 42.6	1.5 ± 0.8

Cell Viability Studies

To preliminarily assess the cellular infiltration and cell growth, NIH 3T3 fibroblasts were used as a model. Figure 28 shows the cell viability results from a 3-day study of CMC/PEO meshes, CMC/PEO meshes with holes, PCL meshes, and PCL meshes with holes. It is clear that CMC/PEO meshes were cytocompatible. However, PCL meshes showed lower cell viability than the control, probably because that 3T3 cells adhere less on the PCL. Most importantly, both meshes with holes exhibited lower cell viabilities than those without holes. The reason is not completely clear, and we are investigating it currently.

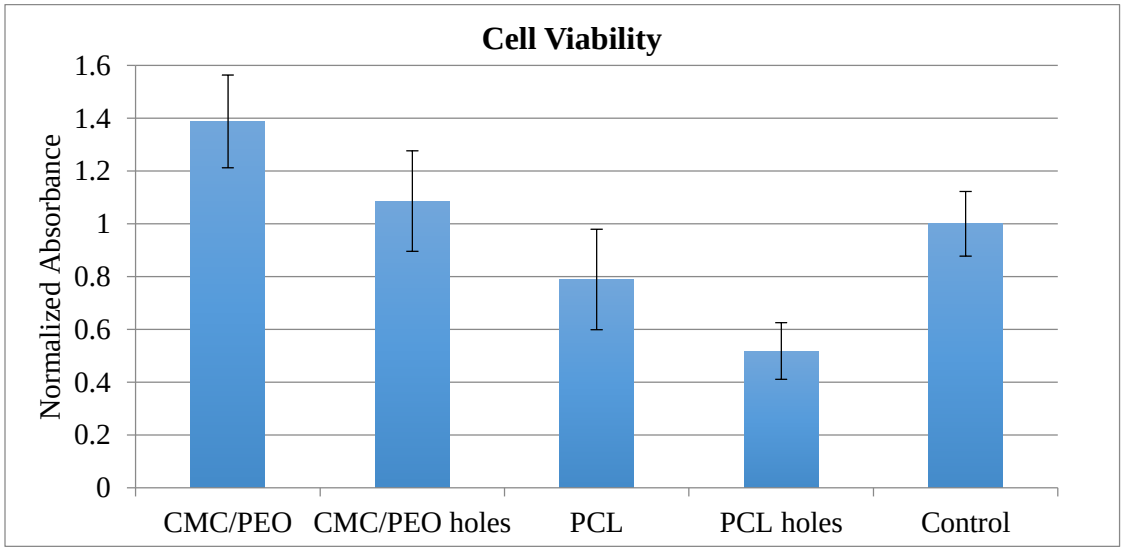

Figure 28: Cell viability study of CMC/PEO and PCL meshes with and without holes

After combining 4 layers together with the use of iCMBA, the cell viability is shown in Figure 29. The results of a 3-day cell viability study of 4-layered (PCL, CMC/PEO, PCL, CMC/PEO) meshes with and without holes demonstrated that with the holes, the cell viability increased. The cell viability is lower than that of the control, due to the toxicity of iCMBA. We are currently changing the amount of iCMBA and periodate to minimize the cytotoxicity.

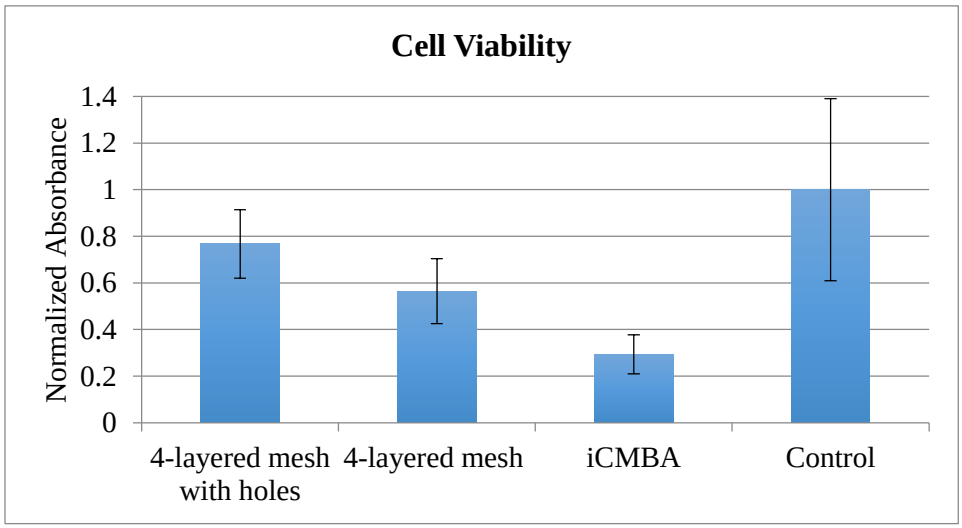

Figure 29: Cell viability study of multi-layered CMC/PEO and PCL meshes and iCMBA

Chapter 4

Discussion and Future Directions

Two different compositions of electrospun fibrous meshes were successfully prepared with micro-patterned holes and bound to create a multi-layered mesh. PCL meshes can provide the mechanical properties that are required in hernia repair. CMC/PEO layers can give better cytocompatibility and increased cell infiltration, since they are semi-soluble in water. The innovative structure enables cell-infiltration into the meshes, leading to a faster integration of the meshes and healing of the wound, while also enabling a progressive mechanical take-over from the meshes to newly regenerated tissue.

First, the factorial analysis determined the ideal electrospinning conditions for CMC/PEO meshes so that the electrospinning of the CMC/PEO meshes could be optimized. The factorial analysis also provided an in-depth understanding of the magnitude of the effect of each key factor on the response factors and the interactions between the key factors. SEM imaging also provided insight into the quality of meshes from each combination of key factors that were electrospun. The results of the factorial analysis, specifically the equations obtained, enable us to fabricate various fibrous meshes in the future according to different application requirements.

A grid of uniformly spaced and sized micro-holes were successfully created on the meshes. The complete puncture through the mesh was confirmed with SEM imaging. This is also an innovative approach to manufacture elecrospun meshes with desired patterns on the surfaces. Diffferent polymeric layers were also bound togerther by applying our bioegradable adheisve material, iCMBA. Although the binding is not ideal at the current stage, we are optimizing the procedure to make a stronger and less toxic binding layer.

The mechanical strength of hernia meshes is vital to their succes in hernia repair. The tensile mechanical testing of the PCL, CMC/PEO, and multi-layered meshes showed that they can be tuned by

different composition and structures. To evaluate the applicability for hernia repair, standard ball bursting tests will be conducted in the future.

The preliminary cell viablity study showed that CMC/PEO meshes supported greater cell proliferation than did the PCL meshes. This supported the hypothesis that CMC/PEO meshes would provide advantageous biological properties for the mesh. However, in the first study, meshes with holes had poorer cell viability than meshes without holes. This was likely due to the punch not being properly sterilized between all uses. Before the 4-layered mesh cell viability study, the punch was sterilized. This study showed that the multi-layered meshes with holes supported greater cell viability than did the multi-layered meshes without holes, as hypothesized. Additionally, the cell viability study showed that iCMBA is cytotoxic and likely responsible for the lesser cell viability of the multi-layered meshes compared to the individual meshes of CMC/PEO and PCL. Future studies should investigate alternative attachment methods to achieve optimal biological propertires for the muli-layered CMC/PEO and PCL meshes.

Overall, a novel biodegradable hernia mesh was fabricated by electrospinning layers of PEO/CMC and PCL and then connecting the layers with iCMBA. The ideal mesh requires not only a soft nature and in vivo biodegradability, but also a gradual transfer of mechanical loads upon implantation to promote healing. The polymers were used for their mechanical and biological properties as to achieve these goals. PEO/CMC provided antibacterial and optimal biological properties. PCL provided faster fabrication of meshes and excellent mechanical properties. A factorial analysis was used to determine the ideal electrospinning conditions for the PEO/CMC meshes. A custom-made hole punch was designed to achieve micro-patterning of the meshes. iCMBA was used to connect mesh layers and achieve a multi-layered scaffold. Together, these two different mesh layers achieved a mesh potentially suitable for use in hernia repair. Further studies should be conducted to further investigate the application of the meshes in hernia repair. In particular, further cell proliferation and penetration studies need to be performed. An animal model should be used and include comparisons with commercially available hernia meshes.

BIBLIOGRAPHY

1. Kingsnorth A, LeBlanc K: Hernias: inguinal and incisional. *Lancet* 362: 1561–71, 2003

2. Engelsman AF, van der Mei HC, Ploeg RJ, Busscher HJ: The phenomenon of infection with abdominal wall reconstruction *Biomaterials* 28: 2314–2327, 2007

3. Franco RA, Nguyen TH, Lee B-T: Preparation and characterization of electrospun PCL/PLGA membranes and chitosan/gelatin hydrogels for skin bioengineering applications. *J Mater Sci Mater Med* 22: 2207–18, 2011

4. Du J, Hsieh Y-L: Nanofibrous membranes from aqueous electrospinning of carboxymethyl chitosan. *Nanotechnology* 19: 125707, 2008

5. Zhang L, Li Q, Qin J, Gu Y: Musculature tissue engineering to repair abdominal wall hernia. *Artif Organs* 36: 348–52, 2012

6. Cassar K, Munro A: Surgical treatment of incisional hernia. *Br J Surg* 89: 534–545, 2002

7. Nienhuijs S, Staal E, Strobbe L, Rosman C, Groenewoud H, Bleichrodt R: Chronic pain after mesh repair of inguinal hernia: a systematic review *Am J Surg* 194: 394–400, 2007

8. Ibrahim AMS, R. Vargas C, Colakoglu Salih, Nguyen JT, Lin SJ, Lee BT: Properties of Meshes used in Hernia Repair: A Comprehensive Review of Synthetic and Biologic Meshes *Reconstr Microsurg*: 83–94, 2015

9. Hollinsky C, Sandberg S: Measurement of the tensile strength of the ventral abdominal wall in comparison with scar tissue *Clin Biomech* 22: 88–92, 2007

10. Gray SH, Hawn MT, Itani KMF: Surgical progress in inguinal and ventral incisional hernia repair. *Surg Clin North Am* 88: 17–26, vii, 2008

11. Greiner A, Wendorff JH: Electrospinning : A Fascinating Method for the Preparation of Ultrathin Fibers Angewandte: 5670–5703, 2007

12. Baker BM, Shah RP, Silverstein AM, Esterhai JL, Burdick J a, Mauck RL: Sacrificial nanofibrous composites provide instruction without impediment and enable functional tissue formation. *Proc Natl Acad Sci U S A* 109: 14176–81, 2012

13. Pham QP, Sharma U, Mikos AG: Electrospun Poly (E -caprolactone) Microfiber and Multilayer Nanofiber / Microfiber Scaffolds : Characterization of Scaffolds and Measurement of Cellular Infiltration: 2796–2805, 2006

14. Mehdizadeh M, Weng H, Gyawali D, Tang L, Yang J: Injectable citrate-based mussel-inspired tissue bioadhesives with high wet strength for sutureless wound closure *Biomaterials* 33: 7972–7983, 201

ACADEMIC VITA

Sara Orr
393 Hannastown Rd
Greensburg, PA 15601
saor68@gmail.com

Education
Bachelor of Science in Bioengineering (Material Science Option)
Schreyer Honors College
The Pennsylvania State University, University Park, PA

Honors and Awards
Recipient, Dean's List (All semesters)
Recipient, Erickson Discovery Grant (2015)
Recipient, Penn State College of Engineering Research Initiative Grant (2014)
Recipient, Best Student Award, MSRC Summer Research Program (2013)
Recipient, Mr. David and Mrs. Kathy Root Research Scholarship (2013)
Recipient, President's Freshman Award (2012)
Recipient, Schreyer Academic Excellence Scholarship (2011-15)
Recipient, National Merit Finalist (2011)

Professional Experience
Engineering Intern
Product Development, AtriCure (Summer 2014)
- Tested cardiac ablation devices to evaluate their safety
- Performed image analysis and statistical analysis for company reports and successful 510(k) FDA submission

Student Researcher
Transformative Biomaterials and Biotechnology Laboratory, Penn State (2013-present)
- Electrospinning multilayered micro-patterned bioscaffolds from polymers to contribute to hernia repair studies for senior honors thesis

Student Researcher
Musculoskeletal Research Center (MSRC), University of Pittsburgh (Summer 2013)
- Quantified the growth factor, soluble collagen, and sulfated glycosaminoglycan content in small intestinal submucosa and urinary bladder matrix hydrogels
- Wrote an abstract that was published in the MSRC annual report and presented work at the MSRC Summer Research Program Annual Symposium

Publications and Papers

Zhiwei Xie, Nikhil V. Aphale, Tejaswi D. Kadapure, Aniket S. Wadajakar, Sara Orr, Dipendra Gyawali, Guoying Qian, Kytai T.Nguyen, Jian Yang. Design of antimicrobial peptides conjugated biodegradable citric acid derived hydrogels for wound healing. ***Journal of Biomedical Materials Research Part A*** 2015, doi: 10.1002/jbm.a.35512 (In press)

Activities

Volunteer, Mount Nittany Medical Center, Emergency Department and Surgical Center (May 2015-present)

Volunteer, Mid-State Literacy Council (April 2015-present)

Mentor, Career Development Program, Schreyer Honors College (2014-present)

International Engineering Student Envoy, College of Engineering (2013-2015)

Recruiting Captain & Squad Leader, Penn State THON Organization Apollo (2011-present)

Member, Global Medical Brigades (2011-12)

Member, Morale Committee, Penn State THON Organization Apollo (2011-12)